Published in final edited form as:
J Comp Neurol. 2010 June 1; 518(11): 2051–2070. doi:10.1002/cne.22321.

Receptive-field Properties of V1 and V2 Neurons in Mice and Macaque monkeys

Gert Van den Bergh[1,2], **Bin Zhang**[1], **Lutgarde Arckens**[2], and **Yuzo M. Chino**[1]

[1]College of Optometry, University of Houston, 505 J. Davis Armistead Bldg., Houston, Texas 77204-2020, U.S.A., Tel.: +1-713-743-1955

[2]Laboratory of Neuroplasticity and Neuroproteomics, Katholieke Universiteit Leuven, Naamsestraat 59, B-3000 Leuven, Belgium. Tel.: +32(16)323929, Fax: +32(16)324598

Abstract

We report the results of extracellular single-unit recording experiments where we quantitatively analyzed the receptive-field (RF) properties of neurons in V1 and an adjacent extrastriate visual area (V2L) of anesthetized mice with emphasis on the RF center-surround organization. We compared the results with the RF center-surround organization of V1 and V2 neurons in macaque monkeys. If species differences in spatial scale are taken into consideration, mouse V1 and V2L neurons had remarkably fine stimulus selectivity, and the majority of response properties in V2L were not different from those in V1. The RF center-surround organization of mouse V1 neurons was qualitatively similar to that for macaque monkeys (i.e., the RF center is surrounded by extended suppressive regions). However, unlike in monkey V2, a significant proportion of cortical neurons, largely complex cells in V2L, did not exhibit quantifiable RF surround suppression. Simple cells had smaller RF centers than complex cells, and the prevalence and strength of surround suppression were greater in simple cells than in complex cells. These findings, particularly on the RF center-surround organization of visual cortical neurons, give new insights into the principles governing cortical circuits in the mouse visual cortex and should provide further impetus for the use of mice in studies on the genetic and molecular basis of RF development and synaptic plasticity.

Keywords

receptive field; center-surround organization; surround suppression; visual cortex; mouse; macaque monkey

INTRODUCTION

The mouse has been extensively used as a preferred model in visual neuroscience to explore the molecular basis of visual cortical development and plasticity during periods of restricted or altered vision (see reviews by Hensch (2005); Callaway (2005); Tropea et al. (2009)). However, information on the quantitatively analyzed receptive-field properties of neurons in the mouse primary visual cortex (V1) are sparse compared to other rodents such as rats (Girman et al., 1999) and squirrels (Heimel et al., 2005; Van Hooser et al., 2005) or highly visual animals including cats and monkeys. Only recently, the availability of transgenic mice and advanced imaging techniques led to renewed interest in the response properties of

Corresponding author: Gert Van den Bergh, Laboratory of Neuroplasticity and Neuroproteomics, Katholieke Universiteit Leuven, Naamsestraat 59, B-3000 Leuven, Belgium. Tel.: +32(16)323929, Fax: +32(16)324598, gert.vandenbergh@bio.kuleuven.be.

mouse visual cortex (Cang et al., 2008; Sohya et al., 2007). The comprehensive study of RF properties of V1 neurons by Niell and Stryker (2008) has unambiguously demonstrated that neurons in mouse V1 exhibit fine selectivity for spatial and temporal frequencies, orientation, and direction of stimulus drift that are generally comparable to tuning in higher species if spatial scales are taken into consideration. With silicon electrode arrays embedded in V1, they were also able to reveal several response properties that are unique to a certain group of V1 neurons (e.g., 'putative' inhibitory neurons) and clear laminar differences in the RF properties of individual neurons.

The objectives of this study were three-fold. First, according to these investigators the standard extracellular microelectrode recording using traditional single metal electrodes is likely to severely bias sampling and therefore, may not be an adequate technique to be employed for studies on signal processing in mice visual cortex. In this study, therefore, we first determined whether the quantitatively analyzed RF properties of mouse V1 neurons, revealed by our standard recording methods using single 'traditional' tungsten-in-glass electrodes, are significantly different from those reported by Niell and Stryker.

In the primate visual brain, the great majority of V1 output is transmitted to V2 for information processing. The majority of primate V2 neurons exhibit monocular and binocular RF properties that are largely similar to those in V1, suggesting that the basic mechanisms controlling information processing are similar in both areas for the majority of neurons (Burkhalter and Van Essen, 1986; Hubel and Livingstone, 1987; Maruko et al., 2008; Sakai et al., 2006; Solomon et al., 2004; Zhang et al., 2005). Although the topographic maps of mouse extrastriate visual areas are well explored (Kalatsky and Stryker, 2003; Wagor et al., 1980; Wang and Burkhalter, 2007), we know nothing about information processing in mouse V2. Therefore, we next examined whether the tuning properties of extrastriate neurons (lateral V2 (V2L)) are similar to those in V1.

Cortical circuits known for mediating suppressive RF surrounds of individual neurons in monkey V1 have been hypothesized to be associated with ocular dominance plasticity in V1 of mice (Hensch, 2005) and kittens (e.g. Trachtenberg et al, (2000)). However, the RF center-surround organization of V1 or V2 neurons has not been explored in mice. Therefore, we measured the receptive-field center and surround sizes, and the strength of surround suppression by obtaining area-summation functions for individual neurons in mouse V1 and in the adjacent V2L. The results in mice were compared with similar data obtained in the same laboratory for macaque V1 and V2. Another motivation for studying the mouse RF center-surround organization was that knowing the nature and the extent of RF surround suppression should give novel information concerning the role of intrinsic long-range connections in mouse visual cortex (Van Hooser, 2007) and/or feedback connections from higher-order visual areas (Angelucci and Bullier, 2003; Bair et al., 2003).

We found that V1 neurons showed fine stimulus selectivity, as reported by Niell and Stryker (2008), and that V2L neurons in mice had RF properties that were similar to those in V1 with few but significant exceptions. Although a larger proportion of units (mostly V2L neurons) in mice did not have quantifiable surround suppression and fewer neurons in mice exhibited robust surround suppression than in monkeys, the basic RF center and surround organization of neurons in mouse V1 was qualitatively similar in both species. These results suggest that the circuitry responsible for the spatial and temporal filter properties and the RF center-surround organization of V1 and V2 neurons is designed with qualitatively similar principles in mouse and monkeys.

MATERIALS AND METHODS

Subjects

All experimental and animal care procedures used in this study were approved by the institutional animal care and use committee of the University of Houston and were in compliance with the *Guiding Principles for Research involving Animals and Human Beings*. Microelectrode recording experiments were conducted in anesthetized mice of the C57Bl/6 strain ranging in age from 3 to 12 months (n = 8) and in anesthetized and paralyzed adult monkeys (*Macaca mulatta*, n = 4). Mice were obtained from Harlan Sprague Dawley Inc. (Indianapolis, IN) and were housed under a conventional 12h light / 12h dark schedule.

Preparation

Mice were anesthetized with urethane (1.5 mg/g body weight, i.p.), and if necessary, additional doses of 4-6 mg urethane were given to induce surgical anesthesia. A tracheotomy was performed and a short plastic tube was inserted into the open end of the trachea, just below the larynx. A larger plastic tube blowing 100% oxygen was placed in front of the opening of the trachea tube enriching the inhaled room air with oxygen. The animal's core temperature was kept at 37.6°C. The animal was mounted in a custom-built stereotaxic frame with the head held in place by two ear bars with fine tips (1.5 mm) and a mouth bar that fixed the upper incisors. Two electrocardiograph leads were inserted subcutaneously at the left and right side of the thorax to monitor the heart rate continuously during the experiment enabling us to assess the depth of anesthesia, which is crucial for obtaining good visual responsiveness. The animal's corneas were protected from drying out by regular application of a 1:1 mixture of mineral oil and Vaseline. With this procedure we could maintain the reasonably good optical quality of the eyes. Since the nictitating membrane in mice does not block the cornea under anesthesia and the residual eye drift following urethane anesthesia (without paralysis) is virtually absent in mice, there was no need to employ special procedures to control these potential issues of their physiological optics. The ipsilateral eye was masked by a black cap over the eyeball and responses were only recorded from the contralateral, right eye. A small (0.5 mm) craniotomy was performed over the left hemisphere over the central region of V1. After the opening was made, the dura mater was locally removed using a sharp scalpel. The exposed brain was covered with a drop of mineral oil to prevent drying. Cardiac or respiratory pulsations of the brain surface could not be observed when making these small craniotomies.

The surgical preparation and recording procedures for the monkey experiments were described in detail elsewhere (Zheng et al., 2007). Briefly, the monkeys were initially anesthetized with an intramuscular injection of ketamine hydrochloride (15 – 20 mg/kg) and acepromazine maleate (0.15 – 0.2 mg/kg). A superficial vein was cannulated and all subsequent surgical procedures were carried out with additional propofol anesthesia (4-6 mg/kg/h, as needed). A tracheotomy was performed to facilitate artificial respiration and, after securing the subjects in a stereotaxic instrument, a small craniotomy and durotomy were made over the lunate sulcus. A small plastic well was placed over the craniotomy and filled with agar and melted wax. After all surgical procedures were completed, the animals were paralyzed by an intravenous infusion of vercuronium bromide (Norcuron; 0.1 mg/kg/h) and artificially ventilated with a mixture of 59% N_2O, 39% O_2 and 2% CO_2. Anesthesia was maintained by the continuous infusion of a mixture of Propofol (4 mg/kg/h) and Sulfentanyl Citrate (0.05 μg/kg/h). Core body temperature was kept at 37.6°C. Cycloplegia was produced by topical instillation of 1% atropine and the animals' corneas were protected with rigid gas-permeable, extended wear contact lenses. Retinoscopy was used to determine the contact lens parameters required to focus the eyes on the stimulus screen. Additional spectacle lenses were also used if necessary.

Recording and visual stimulation

Tungsten-in-glass electrodes were used for isolating the activity of individual cortical neurons. The impedance of our electrode (tip impedance of approximately 1MΩ) was higher than that of the silicon electrodes employed by Niell and Stryker (2008). We found that with our electrodes, we could obtain both good isolation and excellent stability in mouse V1 and V2 (as reported by many investigators in the visual cortex of higher species). The angle of the penetration was about 45° to the surface (see Fig 1) because the vertically oriented electrode entered the surface that had a slope of about 45° around the V1/V2L border. This location of electrode penetration with respect to visual areas was determined according to the published map of V1 and its adjacent visual areas, response properties of neurons and histological examination of electrode tracks (Kalatsky and Stryker, 2003; Wagor et al., 1980; Wang and Burkhalter, 2007).

V1 and V2L classification—For each mouse, we made one or two penetrations and attempted to isolate a unit at about every 50 μm (Fig 1). The majority of the neurons we encountered were located either in the primary visual cortex (V1, Fig 1A) or in the lateral V2 area (V2L, Fig 1B). Due to the anatomical organization of the mouse brain (Kalatsky and Stryker, 2003;Van der Gucht et al., 2007;Wagor et al., 1980;Wang and Burkhalter, 2007) and the angles of our electrode penetrations, i.e., tangential to the cortical surface, if a penetration was made near the border of V1 and V2L, neurons in the deeper layers were identified as those from V2L by histological verification of the recording site (e.g., Fig 1B). For all penetrations, each unit was assigned to either V1 or V2L based on the reconstruction of the recording sites and the location of the V1/V2L border (Fig 1). Specifically, V1 could be distinguished from V2L through its thicker layer IV, its more densely populated layers IV and VI and a sublayer with lower cell density at the base of layer V that is less clear in V2L (van Brussel et al., 2009). Importantly, the detection of the border was based on the sections with a visible electrode track, and because of the occasional difficulty in precisely locating the border on the sections with artifacts from the electrode tracks, we always analyzed a series of adjacent sections, including those that were unaffected by electrode penetrations (Fig 1C,D).

Action potentials were extracellularly recorded and amplified using conventional methods. We searched for well-isolated units and if we encountered multiple units, we discriminated responses from one unit using our standard methods. Our recordings started from the brain surface and ended either when the electrode entered the white matter or the animal's deteriorated physiological situation precluded further recordings. Thus we typically sampled through all layers of cortex with intervals of at least 50 μm between subsequent cells. For mice, the center of the receptive field in the great majority of our units (78%) was located within the central 20° of the center of the visual field, with only a few units as far out as 60°. We did not find any systematic differences in the RF properties of mouse V1 or V2 neurons as a function of eccentricity. This is not especially surprising considering the organization of retina in rodents (Danias et al., 2002; Salinas-Navarro et al., 2009) and the median RF center diameter of cortical neurons in our mice (28° in V1 and 42° in V2L). In monkeys, all receptive fields were located within 6.0° of the projected fovea. There was no systematic difference in their RF properties as a function of eccentricity except for slight increases in the RF center sizes with eccentricity as previously reported (Cavanaugh et al., 2002). Recorded action potentials were digitized at 25kHz, sampled at a rate of 140Hz (7.2 ms bin widths) and compiled into peristimulus time histograms that were equal in duration to and synchronized with the temporal cycle of the grating, by using data acquisition systems (System-II and System-III, Tucker-Davis Technologies, Alachua, FL).

For mice, visual stimuli were generated using custom-developed stimulation software using Matlab (The MathWorks, Natick, MA) and the Psychophysics Toolbox (Brainard, 1997; Pelli, 1997). Stimuli were presented on an LCD monitor (frame rate = 60Hz, mean luminance = 27 cd/m^2, 1280 × 800 pixels, 83° × 61°) at a distance of 25 cm from the eyes either perpendicular to the rostrocaudal axis of the animal for RFs at <30° from this axis, or at an angle of 45° for RFs at >30°. This limited distortion of the visual stimuli for RFs at higher azimuths. For monkeys, visual stimuli were generated on a monochrome CRT monitor (VRG) with ultrashort persistence (frame rate = 140Hz, mean luminance = 50 cd/m^2, 800 × 600 pixels, 20° × 15°) at a distance of 114 cm, using custom made software.

Data analysis

For mice, receptive fields were first mapped on the tangent screen using moving dark edges. The receptive-field properties of individual neurons were quantitatively analyzed by showing drifting sinusoidal gratings that covered the entire monitor (83° × 61°) with a temporal frequency of 3Hz and a contrast of 99%. Stimulus presentations were interleaved with blank gray screens of mean luminance (27 cd/m^2) to determine the spontaneous activity of the neuron. Spontaneous activity was subtracted from visually evoked responses before tuning curves were analyzed. In all tests, stimulus conditions were shown twice for 10 cycles (3s at 3Hz) in random order and interleaved with ≥3s of gray background.

For each unit, the orientation tuning was first determined by showing 12 equally spaced different directions of drifting sinusoidal gratings with a spatial frequency near their optimal (around 0.02 c/d – 0.06 c/d). At the preferred orientation/direction of each cell, the unit's spatial frequency tuning was determined by presenting drifting sinusoidal gratings with 11 different spatial frequencies, ranging from 0.002 c/d to 1.6 c/d. At the optimal orientation and spatial frequency of each unit, we determined the temporal frequency tuning by varying stimulus temporal frequency in 6 steps between 2 and 15Hz. With gratings optimized for the spatial and temporal properties of each unit, its contrast-response function was obtained by varying stimulus contrast between 2.0% and 99%.

To measure the size tuning of the unit, the position of the receptive field center was initially determined using small moving dark edges, fine tuned by locating the position on the monitor screen where a small circular optimized drifting sinusoidal grating (usually around 10° diameter) produced the strongest response. At this position the size tuning experiment was performed by varying stimulus size in 16 steps from 1° to 70° in diameter and keeping all other stimulus parameters optimal for each cell. If the size tuning curve indicated that stimuli were not centered on the receptive field (e.g., the rising portion of the size tuning function was shifted to the right (higher values) on the x-axis and the rising portion of the function had a uncommonly steep slope), we located the central point of the RF center and the size tuning experiment was repeated until we found the exact position of the RF.

The characterization of these receptive field properties for a given unit took about 40 to 60 min. In some cases, units could not be kept stable to complete all measurements (resulting in the number of sample units for various measurements to be different). In some units, the high degree of spontaneous activity, low response rate or intermittent bursting responses precluded an accurate determination of the center of the receptive field, preventing the execution of the size tuning experiment. TF tuning experiments were performed in 5 of the 8 mice.

For monkeys, receptive fields for both eyes were mapped using handheld stimuli and receptive field characteristics were determined by recording responses to high-contrast (80%) sine wave gratings (about 1.0° in diameter) drifted at 3.1 Hz in the unit's preferred direction. Receptive field characteristics were analyzed for both eyes, but the data for the

dominant eye were used for comparisons in this study. Most stimulus paradigms were similar to those of mice, except that 5 cycles of each sinusoidal grating were shown and the recording range for the stimuli was different. For spatial frequency tuning, 12 different stimuli were shown ranging from 0.2 to 16 c/d. Stimulus temporal frequencies ranged from 0.8 to 51.2Hz in octave steps. Contrast was varied between 1 and 80% and stimulus size between 0.13° and 10° in diameter.

Cell classification—Cells were classified as simple or complex on the basis of the temporal characteristics of their response to drifting sine wave gratings of the optimal orientation and spatial frequency (Skottun et al., 1991). For simple cells, the amplitude of the first harmonic component (F_1) was used as the response measure and for complex cells, the amplitude of the DC component (the average discharge rate) was used for all analyses. We used the F_1/F_0 ratio for cell classification, i.e. neurons with a F_1/F_0 ratio > 1 were classified as simple cells and units having the F_1/F_0 ratio < 1 as complex cells. In some cases, we encountered episodic bursting that contaminated the DC component of the cells responses. If clear response modulation in the PSTH was observed, the F_1 component of these cells was then used for further analysis of the units' tuning properties. All curves were fit using a least squares minimalization algorithm.

Orientation tuning—The preferred orientation and bandwidth for each unit was determined by fitting the orientation tuning functions with wrapped Gaussian functions (Swindale, 1998)

$$R(\theta)=m_1\sum_{n=\infty}^{n=\infty}\exp[(\theta - m_2+180n)^2/(2m_3^2)]$$

Where θ is orientation, m_1 is amplitude, m_2 is preferred orientation and m_3 is SD of the Gaussian function. Bandwidth was calculated by measuring the half width at the half height. To determine the unit's selectivity for stimulus orientation/direction we calculated direction and orientation selectivity indices (DSI and OSI). To obtain OSI, we used the following equation,

$$OSI=(R_{pref} - R_{ortho})/(R_{pref}+R_{ortho})$$

where R_{pref} is the peak response in the preferred orientation, and R_{ortho} is the response in the orientation orthogonal to the preferred orientation (Niell and Stryker, 2008). Circular variance (CV) was calculated by the following equation:

$$CV=1(\sum r_k e^{i2\theta k})/\sum r_k$$

where r_k is response amplitude, θ_k is angle ranged from 0 to 360 degree. It is important to note that the orientation tuning properties of a given neuron could differ depending on which of these three methods were employed to analyze our data, i.e., OSI, bandwidth, or circular variance. The orientation selectivity measured with OSI and bandwidth methods is likely to be similar. However, circular variance takes responses of a neuron to all stimulus orientations. Consequently, the orientation selectivity of a cell where the cell has clear peak responses at its preferred orientation but responds with low firing rates to many other orientations tends to give a relatively higher circular variance values. These mild responses at non-preferred orientations do not substantially affect the OSI or bandwidth values in most units while they influence circular variance values.

DSI was calculated from the fitted function using $DSI=(R_{pref} - R_{opposite})/(R_{pref}+R_{opposite})$, where R_{pref} is the response in the preferred drift direction, and $R_{opposite}$ is the response in the opposite direction (Niell and Stryker, 2008).

Spatial frequency tuning—Each cell's optimal spatial frequency, spatial resolution and bandwidth were determined from the fitting of the spatial frequency response data with a Gaussian function (DeAngelis et al., 1993)

$$R(sf)=m_1 \exp[(sf - m_2)^2/(2m_3^2)]$$

where sf is spatial frequency, m_1 is amplitude, m_2 is optimal spatial frequency and m_3 is SD of the Gaussian function. Spatial resolution was determined by locating the highest spatial frequency where the fitted response level dropped to the rate of spontaneous activity. For those units that had no spontaneous activity, we located the highest spatial frequency where the fitted response level dropped to zero.

Based on the fitted function, the left branch of the curve from 1/16 of the optimal spatial frequency to the optimal spatial frequency (optSF) was used to calculate the Low Spatial Frequency Variance (LSFV) by the following equation (Xing et al., 2004):

$$LSFV=\frac{\int_{optSF/16}^{optSF} R(sf) \cdot (\log_{16}(sf) - \log_{16}(optSF))^2 \cdot d\log_{16}(sf)}{\int_{optSF/16}^{optSF} R(sf) \cdot d\log_{16}(sf)}$$

Temporal frequency tuning—The temporal frequency response data were fitted with a Gaussian function described below from which we determined the optimal temporal frequency, temporal frequency resolution and bandwidth (DeAngelis et al., 1993).

$$R(tf)=m_1 \exp[(tf - m_2)^2/(2m_3^2)]$$

where tf is temporal frequency, m_1 is amplitude, m_2 is optimal temporal frequency and m_3 is SD of the Gaussian function. Temporal resolution was determined by locating the highest temporal frequency where the fitted response level dropped to the rate of spontaneous activity.

Contrast sensitivity—Contrast response curves were fitted with the nonlinear Naka-Rushton equation (Albrecht and Hamilton, 1982; Naka and Rushton, 1966)

$$R(C)=gC^n/(C_{50}^n+C^n)$$

where g is the gain, C_{50} the contrast at mid-saturation and n the exponent. To prevent overestimation of the contrast sensitivity of the unit, responses that were lower than 2 times the standard error of the spontaneous activity level after subtracting the spontaneous activity were assigned to zero, before fitting with the Naka-Rushton equation.

Size tuning—Size tuning curves were fitted with the following formula (Cavanaugh et al., 2002; Zhang et al., 2005): $R(x) = K_c L_c(x)/[1 + K_s L_s(x)]$; $L_c(x) = [w_c \times \mathrm{erf}(x/w_c)]^2$; $L_s(x) = [w_s \times \mathrm{erf}(x/w_s)]^2$. x is the stimulus diameter, K_c and K_s are the gains of the center/surround, and L_c and L_s are the summed squared activities of the center/surround mechanisms. The

spatial extents of the center/surround components are represented by w_c and w_s. During curve fitting we always constrained functions so that $w_c < w_s$. Based on the area-response function of each unit, we determined the extent and size of the *RF center*, defined as the area in which the smallest circular grating produced the maximum response. The *RF surround* size was determined by locating the point in the fitted function at which further increases in stimulus diameter did not alter response amplitude, i.e., at the asymptote response (Fig 6C). The asymptotic point was defined as the point of the function where a one-degree increment of stimulus diameter failed to alter the response rate by 5%. The suppression index (SI), which expresses suppression as a fraction of the peak firing rate, was calculated from the fitted curve with the following equation:

$$SI=(R_{opt} - R_{supp})/R_{opt}$$

where R_{opt} is the peak response rate and R_{supp} is the response rate at the outer edge of the RF surround, i.e., beyond which stimulation with larger stimuli does not significantly change the response rate.

Statistics—Because the majority of response properties were not normally distributed, we used median values to evaluate overall tuning and Kruskal-Wallis rank test was applied in order to test the significance of differences unless specified otherwise.

Histology

At the end of each penetration, two small electrolytic lesions (10s, 5μA, electrode negative) were made along the electrode track. The animals were given an overdose of sodium pentobarbital (Nembutal) and perfused transcardially with 0.1M phosphate buffered saline (PBS, pH 7.4) followed by 4% paraformaldehyde. For monkeys, frozen sections were made, while for mice 50μm-thick Vibratome sections were cut, and stained with Nissl substance following standard procedures. Photographs of the histological patterns were obtained with a Zeiss Axio-Imager equipped with a Zeiss Axiocam. Brightness and contrast were adapted using Adobe Photoshop CS2. Recording sites were reconstructed based on the position of the electrolytic lesions and the recording depths along the electrode track (Fig 1).

RESULTS

We quantitatively analyzed the receptive-field properties of 96 neurons (69 in V1 and 27 in V2L) in 8 mice. In addition, we obtained comparable data from 203 units (96 in V1 and 107 in V2) from 4 macaque monkeys in order to gain insights into possible species differences in the RF center-surround organization. While these results on the RF center-surround have not been published, the data from monkeys on the orientation/direction selectivity, the spatial and temporal frequency tuning properties and contrast sensitivity have been published elsewhere (Maruko et al., 2008; Zheng et al., 2007)(see Table 1 for summary).

Each neuron was classified as a simple or complex cell on the basis of the temporal characteristics of their responses to drifting sine wave gratings of the optimal orientation and spatial frequency, i.e., by calculating F_1/F_0 response ratios (Skottun et al., 1991). The distribution of F_1/F_0 ratios was bimodal for V1 as reported in other rodents and higher mammals (Fig 2A). However, in V2L, only 4 out of 27 units (15%) were classified as simple cells (F_1/F_0 ratios >1.0) whereas 26 out of 69 units (38%) in V1 were identified as simple cells (Fig 2A). The proportion of V1 simple cells in this study was lower than that reported by Niell and Stryker (2008) (49%), but higher than the ratio found in V1 of grey squirrel (26%) (Heimel et al., 2005). The difference in the proportion of simple vs. complex cells between V1 and V2L is significant (Chi-square test, $p < 0.03$). Although the median F_1/F_0

ratio of V1 neurons in layer IV was higher than those in layers II-III or layers V-VI, these differences were not statistically significant (Fig 2B).

Spatial and temporal tuning and contrast sensitivity

The neuron's selectivity to stimulus orientation, spatial frequency, temporal frequency and contrast were quantitatively determined using drifting sinusoidal gratings that extended over the entire screen from which the optimal stimulus values were extracted for each unit. Figure 3 illustrates representative tuning functions of V1 and V2 neurons for stimulus orientation, spatial and temporal frequency and contrast. These cortical neurons were remarkably well tuned to each stimulus parameter and the tuning characteristics were remarkably similar between V1 and V2.

Orientation/direction selectivity—To analyze orientation/direction selectivity across our cell population, we calculated the orientation selectivity index (OSI) and direction selectivity index (DSI)(Niell and Stryker, 2008). The overall selectivity for stimulus orientation was quite high in V1 as reported by Niell and Stryker (2008), and the median OSI was similar for V1 and V2L neurons (0.90 for V1 and 1.0 for V2L) (Fig 4A). The range of orientation bandwidth (half-width at the half-height) was broad for both V1 and V2L neurons, spanning from only several degrees to over 90 degrees. The median bandwidth (half width at half height) was relatively narrow for both V1 (21.3°) and V2L units (14.6°) (Fig 4B). The average bandwidth of orientation selective V1 units (22.2°) was similar to the mean value found by Niell and Stryker (2008). Although some units showed elevated responses to one direction and not to an opposite direction, the median DSI was rather low (Fig 4C), indicating that most units were not sensitive to the direction of stimulus drifts. The distribution here is similar to that reported by Niell and Stryker (2008). The median DSI for V1 units (0.22) was better than that for V2L units (0.16) but this difference was not statistically significant ($p > 0.4$). Importantly, there were no significant differences in orientation/direction tuning between V1 and V2L neurons.

Spatial frequency—Our population analysis on the SF tuning showed that the median optimal SF for V1 units (0.04 c/d) was similar to that of V2L units (0.03 c/d)(Fig 4D). Also the median spatial resolution of V1 units (0.15 c/d) was similar to that for V2L neurons (0.13 c/d) (Fig 4E). Although some neurons responded preferentially to lower spatial frequencies, these neurons were relatively well tuned and displayed band-pass characteristics (Fig 4F). Only 29% of all units were classified as 'low-pass' units. The median bandwidth for V1 neurons was 2.97 octaves while it was 2.48 octaves for V2L neurons. The difference was not statistically significant ($p = 0.30$). The mean optimal SF (0.04 c/d) and bandwidth (2.38 octaves) of V1 units were nearly identical to those previously reported (Niell and Stryker, 2008).

As in monkey V1, the SF bandwidth was strongly correlated with the low spatial frequency variance (LSFV) of V1 and V2L neurons, a measure of the degree of response attenuation at lower spatial frequency (Xing et al., 2004) (Fig 5A). Importantly the LSFV values are also correlated with circular variance, a measure of global orientation tuning of simple and complex cells (Fig 5B). These results suggest that 'global' inhibition plays a significant role in spatial frequency and orientation tuning of neurons in mouse V1 and V2L, as suggested for macaque V1 (Xing et al., 2004).

Temporal frequency—The median optimal temporal frequency was 3.4 Hz for V1 units and 3.0 Hz for V2 neurons (Fig 4G). This small difference between V1 and V2L was not significant ($p > 0.2$). Interestingly, the median temporal resolution of V2L neurons (24.9 Hz) was significantly higher than that for V1 neurons (12.2 Hz)($p = 0.01$). The temporal

resolution of V1 neurons was similar to but lower than the median temporal high-frequency cut-off of grey squirrels (Heimel et al., 2005) or rats (Girman et al., 1999). A relatively large proportion (37%) of all units exhibited low-pass tuning characteristics because their responses did not drop below half the maximum firing rate at the lowest temporal frequency tested (2 Hz). More importantly, 75% of V2L units had low pass tuning. The prevalence of low-pass cells might have been less if we used stimuli with lower temporal frequencies. *Among units with 'band pass' tuning*, the mean bandwidths were 1.97 octaves for V1 and 1.71 octaves for V2L neurons, and there was no statistical difference between V1 and V2L ($p > 0.7$)(Fig 4I). However, if units with a low-pass characteristic are included in these comparisons, there was a significant difference between V1 and V2L ($p < 0.04$).

Contrast—All contrast versus response data could be adequately fitted with a Naka-Rushton equation (a hyperbolic function). The C_{50} of this equation is the mid-saturation contrast, reflecting the overall sensitivity of the unit to stimulus contrast while the exponent *n* indicates the steepness of the function. The contrast sensitivity is the reciprocal of threshold stimulus contrast at which a unit still fired above the spontaneous firing plus two standard errors. Both the C_{50} and contrast sensitivity of these units indicated that neurons in mouse visual cortex require high contrast gratings to reliably initiate responses above noise. The median C_{50} was 49.0% for V1 units and 53.9% for V2L neurons while the median contrast sensitivity was 4.1 for both V1 and V2L (Figs 4J and 4L, respectively). The range of C_{50} and contrast sensitivity among units was large, e.g., contrast sensitivity ranged from very sensitive (sensitivity > 100) to nearly insensitive (sensitivity < 2, indicating a contrast threshold > 50%). While the majority of V1 and V2L units had C_{50} values in a higher range, up to 26% of both V1 and V2 units were observed having a $C_{50} > 100\%$ (i.e., showing no signs of saturation). For the calculation of the median C_{50} values, these units were excluded.

The median slope of the contrast response functions (the exponent *n*) was 1.9 for V1 units and 2.4 for V2L neurons (Fig 4K). The spread of exponent values was very large, with a sizeable number of units with exponent > 10, indicating that these units did not exhibit contrast saturation. There were no significant differences between V1 and V2L ($p > 0.3$). The C_{50}, n, and sensitivity values of V1 neurons were generally similar to those for rat and grey squirrels (Girman et al., 1999;Heimel et al., 2005). However, the C_{50} value of mouse V1 reported by Niell and Stryker (2008) was about one-half of the median C_{50} of this study. Taken together, our data in mouse V1 were generally consistent with the comparable data from the previous studies in mice, rats and squirrels, and the temporal resolution was the only tuning property that significantly differed between V1 and V2L in mice.

Simple vs. complex cells—Next, we asked whether these tuning properties differ between simple and complex cells in V1 and V2L because this issue has never been explored in mouse V1 (Fig 6). Since there were only 4 simple cells in V2L, we did not segregate V1 and V2L data. Although there were small differences in several tuning properties (e.g., OSI, DI, SF bandwidth, optimal TF, TF bandwidth, C_{50}, and contrast sensitivity), none of these differences reached statistical significance except that the optimal spatial frequency and the spatial resolution of complex cells were significantly higher than V1 simple cells ($p < 0.05$).

Layer differences—Previous studies of rodent's V1 reported that many response properties of individual neurons vary considerably between the upper (II-III) and the lower (V-VI) layers (Girman et al., 1999; Heimel et al., 2005; Niell and Stryker, 2008). Therefore, we segregated V1 units into three groups (the most frequently employed method in the literature), those belonging to layers II - III, layer IV, and layers V - VI, and compared the tuning properties (Fig 7). Despite some mild layer differences that are consistent with

previous reports (e.g., OSI, orientation bandwidth, and SF bandwidth), there were no significant differences for any RF property.

Spontaneous activity, peak firing rate and tuning properties—The spontaneous and peak firing rates of our V1 and V2L units were substantially higher than those previously reported for rodents (e.g. (Girman et al., 1999; Heimel et al., 2005; Niell and Stryker, 2008))(Figs 7G, 7H, 8A and 8B). It is important to note that the peak firing rate here, as in all other measurements of tuning properties, represents the response rate after subtracting spontaneous firing rate from the recorded response rate for each unit. In contrast to the previous studies in mice, rats, and squirrels where neurons in the upper layers have lower spontaneous firing rates than in the lower layers, we did not find similar layer differences (Fig 7G). Therefore, we first compared the peak firing rate of each cell as a function of its spontaneous firing (Fig 8C). We found a relatively strong correlation between the peak firing rate and noise ($r = 0.71$, $p < 0.001$). Thus, signal processing was not likely to have been affected by the presence of moderately high spontaneous activity. To further examine the effects of spontaneous activity, we compared the tuning properties of neurons as a function of their spontaneous activity level. Each neuron was divided into three categories according to its spontaneous firing (SP), *low SP* (SP < 1.0/spike/sec), *Medium SP* (1.0 < SP < 10 spikes/sec), and *High* SP (> 10 spikes/sec). The median tuning properties are illustrated for each of the three categories of neurons in Fig 8D-O. Except for DSI in V1, there was no significant difference in tuning properties between cells with low, medium, and high spontaneous activity.

Size tuning and RF center-surround organization

We characterized the receptive-field center-surround properties of V1 and V2 neurons by measuring the response amplitude of each unit as a function of the diameter of drifting sinusoidal gratings optimized for orientation and spatial frequency. Stimulus contrast was kept at 99% and temporal frequency was set at 3 Hz. The results from mice were compared to those obtained in 4 macaque monkeys. The data on the area summation functions for monkey V1 (n = 96) and V2 (n = 107) were newly acquired and were never used in any previous publications although similar data were published in separate publications (Zhang et al., 2005). Units in monkey V1 and V2 were encountered around the V1 and V2 border posterior to the lunate sulcus and their RFs were located within 6° of the foveal representation. Size tuning functions were fitted with a ratio of Gaussians (Cavanaugh et al., 2002).

The most important discovery was the overall similarity in the RF center-surround organization of V1 neurons between mice and monkeys. Figure 9 illustrates examples of the size tuning functions of V1 (Fig 9A-D) and V2 (Fig 9E-H) neurons from mouse and monkey. In V1 and V2 neurons of both species, the discharge rate was very low for the smallest patches and monotonically increased with expansion of stimulus diameter, up to a point beyond which further increases in stimulus diameter resulted in suppression of the center responses (e.g. Fig 9A) or in further increase of neuron's response rate (e.g. Fig 9B). In some units in mice, responses kept increasing with stimulus diameter up to the largest stimuli we could present (70°). However, we encountered more units that exhibited clear surround suppression than those without surround suppression in both mice and monkeys.

RF center size—The RF center size (diameter) in mice was about 20-30 times larger than in monkeys. The median RF center size in monkeys was 1.29° for V1 and 1.58° for V2 neurons, while the median center size in mice was 28.9° for V1 and 41.9° for V2L units (Fig 10A and 10E). The differences in the RF center size between V1 and V2 in mice and monkeys were significant ($p < 0.02$ for mice and $p < 0.01$ for monkeys). Interestingly the

difference in RF center size between simple and complex cells was much greater in mice than in monkeys (Fig 11A and 11E). The median center size for simple cells in mice was 21.3° whereas for complex cells it was 37.0°. This difference was significant ($p < 0.001$). In monkey V1, the median center size for simple cells was 1.18° and it was 1.3° for complex cells ($p = 0.9$).

RF surround size—In those units that had a suppression index (SI) greater than 0.10, we determined their surround sizes. The median RF surround size was over 10 times larger in mice than in monkeys. Specifically, the median surround size of V1 neurons in mice was 92.5° and it was 93.3° for V2L neurons compared to 8.3° for V1 and 7.56° for V2 in monkeys (Figs 10B and 10F). The median surround size for simple cells was 90.9° while it was 94.2° for complex cells in mice compared to 8.3° for simple and 7.6° for complex cells in monkeys (Fig 11B and 11F). Note that the surround size for mice was estimated from fit functions up to 100° in diameter and that over 40% of all units from mice had no measurable RF surround.

Although the RF center and surround sizes were very large in mice, species differences in the proportionality of surround versus center size were not as large as differences in measured absolute size values (Figs 10D and 10H). Specifically, we found that the median surround/center ratio was 3.27 for V1 and 2.67 for V2L in mice, whereas the median ratio in monkeys was 5.86 for V1 and 4.43 for V2. Interestingly, the median surround/center size ratio in mice was 3.37 for simple cells and 3.05 for complex cells, whereas in monkeys the median ratio was 5.86 for simple cells and 5.77 for complex cells. The largest surround / center ratio were 7.51 for mice and 21.04 for monkeys. The range of the surround/center ratios was far greater in monkeys than in mice largely because there were many more units with very high ratios (e.g., ratios > 10) in monkeys than in mice (Fig 10H). Those units in monkeys with very high surround/center size ratios and large SI values were V2 neurons that had very small RF centers with exceptionally large surrounds and nearly complete surround suppression ($SI > 0.9$)(e.g., ‘special units’ in Zhang et al. (2005)). These differences between the two species appear to reflect the species difference in their retinal organization (i.e., fovea in monkeys vs. crude retinal streak in mice).

Surround suppression—The overall strength of surround suppression in mice was not as strong as in monkeys (Fig 10C and 10G). Only 16% of all units in mouse visual cortex, compared to 57% in monkeys, exhibited moderate to strong surround suppression ($SI \geq 0.5$). More importantly, there was a clear-cut difference in the strength of surround suppression between V1 and V2 in mice (Fig 10C) while we did not find similar differences between V1 and V2 in monkeys (Fig 10G). Also simple cells in mouse visual cortex (median SI = 0.38) had much stronger surround suppression than complex cells (median SI = 0.11)(Fig 11C and 11D). This difference was statistically significant ($p < 0.001$). In monkeys, there were no differences in median SI between simple cells (0.62) and complex cells (0.59). The differences in SI values between mice and monkeys were highly significant for both simple and complex cells ($p < 10^{-4}$).

In monkey V1 and V2, neurons with smaller RF centers are likely to exhibit a higher degree of surround suppression and there was moderate negative correlation between the RF center size and the strength of surround suppression both in mice ($r=0.63$) and monkeys ($r = 0.50$) (Fig 12A). The strength of surround suppression was mildly but positively correlated with surround size both in mice ($r = 0.45$) and monkeys ($r = 0.47$)(Fig 12B). Importantly, there was a strong positive correlation between the strength of surround suppression and the surround/center size ratio of individual neurons that was qualitatively similar in mice ($r = 0.73$) and monkeys ($r = 0.80$)(Fig 12C). These results reinforce the notion that the RF center-surround organization of V1 and V2 neurons in mouse and monkey visual cortex is

fundamentally similar except for the strength (and the presence/absence) of surround suppression.

Layer differences—For both mice and monkey, we compared the center-surround organization of V1 and V2 units across three groups, those belonging to layers II - III, layer IV, and layers V - VI (Fig 13). While in monkeys, some center-surround properties were clearly different from layer to layer (surround/center size ratio in V1 and V2, $p < 0.01$; center and surround size in V2, $p < 0.05$; suppression index in V1, $p < 0.05$), no significant differences were observed in mouse V1 or V2L, with the exception of a somewhat larger center size in the upper layers of V1 ($p < 0.05$).

DISCUSSION

The most important finding of this study was that the receptive-field center-surround organization of V1 neurons in mouse visual cortex is *qualitatively* similar to that in macaque monkeys. We found that the majority of V1 neurons have a large area outside of the classic RF where stimulation causes suppression of the RF center responses. As in higher species (e.g. (Cavanaugh et al., 2002; Walker et al., 2000), the RF center and surround mechanisms can be well described by a ratio of Gaussians (Cavanaugh et al., 2002). Another important finding was that the RF properties of V2L neurons in mice were qualitatively similar to those in V1, paralleling the overall similarities in the RF properties of macaque V1 and V2 neurons (Maruko et al., 2008; Zhang et al., 2005; Zheng et al., 2007). The notable difference between the two species was that unlike in the primate V2, the RF surround of V2L neurons in mice was much weaker or absent in the great majority of our sample neurons, and that the proportion of simple cells was remarkably low in V2L.

Comparison with previous studies in rodents and methodological consideration

Comparison to previous studies in mice—Despite substantial differences in recording methods, the results of this study mostly agree well with the findings from the recent comprehensive study that uncovered remarkably sharp tuning of mouse V1 neurons (Niell and Stryker, 2008). As briefly mentioned in the result section, the RF size is very similar between the two studies (see below). The overall orientation tuning (OSI or bandwidth) was nearly identical between the two studies. The median optimal spatial frequency for our population of cells are very similar to that in mouse V1 (Niell and Stryker, (2008) and the mouse LGN (Grubb and Thompson, 2003), and the spatial frequency bandwidth in this study was comparable to the bandwidth reported by Niell and Stryker.

However, there were notable differences in some RF properties between this and previous studies. For example, the study by Niell and Stryker revealed many qualitative differences in tuning properties between V1 units in layer 5 and those from other layers. We did not find similar differences although the great majority of neurons in our layers V-VI came from layer V (Fig 7). It is worthwhile to note that the nature and extent of laminar differences in tuning properties vary widely between species, and also within species in different studies (Heimel et al., 2005;Van Hooser, 2007). For example, the spontaneous firing rate of this study was considerably higher than that in mice (Niell and Stryker, 2008) or in grey squirrels (Heimel et al., 2005), but similar to that in rat V1 (Girman et al., 1999). The optimal temporal frequency in this study (3.0-4.3 Hz) was moderately higher than the peak temporal frequency (1.5-2.0 Hz) found in V1 (Niell and Stryker, 2008), lower than in grey squirrels (5.3 Hz) (Heimel et al., 2005), but was similar to that in rat V1 (Girman et al., 1999) and the LGN neurons in mice (Grubb and Thompson, 2003).

Importantly we observed significantly higher C_{50} values (median C_{50} = 39.8% − 46.3%) than earlier studies in mouse V1 (around 20%)(Niell and Stryker, 2008), in squirrel V1

(35%)(Heimel et al., 2005) or dLGN (also around 35%)(Grubb and Thompson, 2003), but our values on C_{50} were similar to the mid-saturation value found in rat V1 (Girman et al., 1999). Moreover, about 26% of all mouse units exhibited no saturation (100% in Fig 4J and 6J). This represents a novel finding in that V1 units exhibiting no or little contrast saturation are very rare in cats and monkeys (e.g., (Ohzawa et al., 1985; Sclar et al., 1990; Zheng et al., 2007), while they are commonly found in the LGN of these animals (Ohzawa et al., 1985; Sclar et al., 1990).

The source of the apparent differences in C_{50} for mouse V1 is unclear. The data on C_{50} in Niell and Stryker's study were based on a much smaller sample size (n = 32) than ours (n = 97) and our data showed a wider range of C_{50} values. Moreover, the higher C_{50} values of our V1 units would predict lower n values (the slope of the contrast-response functions). However, the median n-value of V1 in this study was 2.21, which is nearly identical to 2.4 in Neill and Stryker's study. Another unusual nature of their data on contrast sensitivity is that their median C_{50} (19.8%) is nearly identical to the median C_{50} value (18.6%) we found for macaque V1 (Zheng et al., 2007). This implies that mouse V1 is as sensitive to stimulus contrast as macaque V1. Considering the qualitative differences in the anatomy and functional organization of the retina between mice and monkeys described earlier, these similarities in contrast sensitivity of V1 for the two species are difficult to explain.

Finally, despite substantial differences for a couple of response properties between this and previous study in mouse V1 (e.g., contrast and spontaneous activity) and many advantages of employing the multielectrode array to study information processing in mouse V1, the present study demonstrated that the use of single metal electrodes in a conventional extracellular single-unit recording setup is more than adequate to generate useful data for developmental and other studies on information processing in mouse visual cortex.

Comparisons of stimulus selectivity between mice and monkeys

What can we conclude regarding the information processing of V1/V2 neurons between mice and monkeys? Table 1 summarizes the mean (± se) values of the major RF tuning properties of V1 and V2 neurons for the two species. As expected, a robust species difference was found for the optimal spatial frequency and spatial resolution. Another obvious species difference was found for contrast sensitivity both in V1 and V2. As will be discussed below robust quantitative species differences were found for the center-surround organization. However, the spatial frequency bandwidth, expressed in relative term (octaves), was similar for both V1 and V2 in these two species. Also the orientation bandwidth was similar in mice and monkeys. These relatively fine orientation and spatial frequency tuning properties of mouse V1 neurons raise an interesting point. Rodent's V1 is known to lack the kind of columnar organization that is present in cats and monkeys (Antonini et al., 1999;Hubener, 2003). This appears to suggest, therefore, that the orientation and spatial frequency columns may not significantly contribute in determining the degree of tuning in individual neurons. However, the more subtle contributions of intrinsic long-range axons in e.g. cats and monkeys that interconnect the orientation columns of similar preferred orientations have been amply demonstrated (Bosking et al., 1997;Gilbert and Wiesel, 1989).

RF center-surround organization of V1 and V2 neurons in mice and monkeys

The present study represents the first and only attempt to characterize the tuning properties of V2 neurons and the RF center-surround organization of V1 and V2L neurons in mice. Neurons that exhibit 'length-summation', 'end-stopping', and length tuning have been qualitatively described in squirrel (Van Hooser et al., 2006) and rat V1 (Girman et al., 1999). We found overall similarities in the center-surround organization of V1 neurons between mice and macaque monkeys if spatial scales are taken into consideration.

Center size—The RF center sizes found in this study (median size of 21.3° for simple and 37.0° for complex cells) are generally similar to that reported by Wang and Burkhalter (2007) (mean size of around 20°), but *appear* to be much larger than that reported by Niell and Stryker (2008) for V1 (mean size between 5° and 12° depending on cortical layers with the overall mean size of about 7°). However, if the RF center size reported by Niell and Stryker (2008)(i.e., *'radius at half-height for the Gaussian fit response profile'*) were to be multiplied by a factor of 4 in order to make measurements in these studies 'comparable', that would bring the mean center size of V1 neurons in their study to about 28° in diameter. Thus, the center sizes reported in the two studies are consistent. Interestingly, all earlier studies where classic RFs were mapped for V1 units with hand-held stimuli reported considerably smaller RF sizes than those described above (Drager, 1975; Mangini and Pearlman, 1980; Metin et al., 1988; Simmons and Pearlman, 1983). However, the RF size, determined qualitatively by hand-held stimuli, is known to be much smaller than that measured with drifting sine wave gratings in monkeys ((De Valois et al., 1985) and in cats (Walker et al., 2000).

Surround size and suppression—One of the more obvious differences between mice and monkeys was that slightly over 40% of units in mice (mostly complex cells), as opposed to only 4% in monkeys, did not have suppressive surrounds, and the median size of suppressive surround in both simple and complex cells in mice had diameters exceeding 70°. Many of those units with no surround in our study were identified as V2L neurons (Fig 1). This finding in V2L neurons in mice is very different from the RF surround of V2 neurons in macaque monkeys where surround suppression is highly prevalent and robust (Zhang et al., 2005). It is important to remember that because of the limitation imposed by the size of our monitor screen (83° × 61°), we could not determine the surround size beyond 100° even using our fit area summation functions. Consequently, the surround size and the strength of surround suppression (SI) in mouse visual cortex, in particular for V2L, might have been underestimated. Nevertheless, the surround size was mildly correlated with suppression index and the level of this correlation was similar to that found for monkey V1 and V2. It should be noted that the median center and surround sizes of primate V1 and V2 neurons of this study are slightly larger than those of published data (e.g., (Cavanaugh et al., 2002;Solomon et al., 2004;Zhang et al., 2005)), the small differences may reflect differences in anesthesia, sampling of units, and/or the method to determine the RF center and surround sizes.

What are the anatomical substrates for the RF surrounds in mouse V1 that support such large RF surrounds? In monkey V1, both the intrinsic long-range horizontal connections in V1 and the feedback connections from extrastriate areas (where individual neurons have increasingly larger RFs) are thought to contribute to the surround size and the strengths of surround suppression in V1 neurons (Angelucci et al., 2002; Bair et al., 2003; Schwabe et al., 2006). There is little information in the literature on either the long-range horizontal connections within mouse V1 or the feedback connection to V1 from extrastriate cortex. However, because the average RF size of neurons in mouse extrastriate areas (as determined by hand mapping) are 1.5 to 4 times larger than that in their V1 (Wang and Burkhalter, 2007), the feedback connections from mouse extrastriate neurons could support the suppressive RF surrounds of many V1 neurons in this study. For example, the average size of RFs in area LM lateral to V1, which corresponds to a sub-region of V2L initially defined by Rosa and Krubitzer (1999) and, later, by Kalatsky and Stryker (2003), is about 1.5 times larger than the average size in V1 (Wang and Burkhalter, 2007). Therefore, LM neurons could provide suppressive feedback signals to V1 neurons with relatively smaller RF centers in this study. Also suppressive influence of the LM feedback connections on V1 has been recently suggested for mice (Dong et al., 2004).

With respect to the long-range horizontal connections within V1, the horizontal connections in squirrel V1 are not 'patchy' as in higher mammals, but extend about 1 – 2 mm over cortical space (Van Hooser et al., 2006). This is similar to the distance described for rat V1 (Burkhalter, 1989; Johnson and Burkhalter, 1997). Moreover, the responses of these neurons in squirrels show length summation in 42% of units and 'end-stopping' properties in 16% of all units studied (Van Hooser et al., 2006; Van Hooser and Nelson, 2006). Whether these RF properties reflect the involvement of the intrinsic horizontal connections and/or feedback connections is unclear. In our study, 40% of cortical neurons in mice had 'area summation' with no surround inhibition and the remaining 60% exhibited a broad range of surround suppression. Finally, the ratio of RF surround size over RF center size in each unit was well correlated with the strength of its surround suppression and this relationship was similar in mice and monkeys. This result suggests that the cortical circuits supporting the RF center-surround organization of visual cortical neurons are similar in these two species.

Taken together, despite being a nocturnal creature with relatively small visual cortex and having poor visual acuity (Prusky et al., 2000), the processing of visual stimuli by individual neurons of mouse visual cortex appears to be guided by similar fundamental principles as in animals with higher visual needs. As we described above, there were significant quantitative differences in the strength of surround suppression. However, the qualitative similarities in the RF center-surround organization of V1 neurons between mice and macaque monkeys that we found in this study provide further justification for the use of mice as an animal model to study the molecular basis of synaptic plasticity in developing visual brain, in particular, the study of the cortical mechanisms that regulate the timing of the critical period by modulating the balance between cortical inhibition and excitation (e.g. (Hensch, 2005; Hensch et al., 1998; Morishita and Hensch, 2008; Trachtenberg et al., 2000)).

Acknowledgments

We thank Inge Van Der Auwera for expert technical assistance.

Support: GVDB is a postdoctoral fellow of the Fund for Scientific Research (FWO-Flanders), Belgium and is supported by a travel grant from the same organization. This work was supported by the research grant from National Eye Institute (RO1 EY-008128 to YMC) and Core Grant (RR-07751). YMC is also supported by Benedict-McFadden Professorship.

References

Albrecht DG, Hamilton DB. Striate cortex of monkey and cat: contrast response function. J Neurophysiol. 1982; 48(1):217–237. [PubMed: 7119846]

Angelucci A, Bullier J. Reaching beyond the classical receptive field of V1 neurons: horizontal or feedback axons? J Physiol Paris. 2003; 97(2-3):141–154. [PubMed: 14766139]

Angelucci A, Levitt JB, Lund JS. Anatomical origins of the classical receptive field and modulatory surround field of single neurons in macaque visual cortical area V1. Prog Brain Res. 2002; 136:373–388. [PubMed: 12143395]

Antonini A, Fagiolini M, Stryker MP. Anatomical correlates of functional plasticity in mouse visual cortex. J Neurosci. 1999; 19(11):4388–4406. [PubMed: 10341241]

Bair W, Cavanaugh JR, Movshon JA. Time course and time-distance relationships for surround suppression in macaque V1 neurons. J Neurosci. 2003; 23(20):7690–7701. [PubMed: 12930809]

Bosking WH, Zhang Y, Schofield B, Fitzpatrick D. Orientation selectivity and the arrangement of horizontal connections in tree shrew striate cortex. J Neurosci. 1997; 17(6):2112–2127. [PubMed: 9045738]

Brainard DH. The Psychophysics Toolbox. Spat Vis. 1997; 10(4):433–436. [PubMed: 9176952]

Burkhalter A. Intrinsic connections of rat primary visual cortex: laminar organization of axonal projections. J Comp Neurol. 1989; 279(2):171–186. [PubMed: 2913064]

Burkhalter A, Van Essen DC. Processing of color, form and disparity information in visual areas VP and V2 of ventral extrastriate cortex in the macaque monkey. J Neurosci. 1986; 6(8):2327–2351. [PubMed: 3746412]

Callaway EM. A molecular and genetic arsenal for systems neuroscience. Trends Neurosci. 2005; 28(4):196–201. [PubMed: 15808354]

Cang J, Niell CM, Liu X, Pfeiffenberger C, Feldheim DA, Stryker MP. Selective disruption of one Cartesian axis of cortical maps and receptive fields by deficiency in ephrin-As and structured activity. Neuron. 2008; 57(4):511–523. [PubMed: 18304481]

Cavanaugh JR, Bair W, Movshon JA. Nature and interaction of signals from the receptive field center and surround in macaque V1 neurons. J Neurophysiol. 2002; 88(5):2530–2546. [PubMed: 12424292]

Danias J, Shen F, Goldblum D, Chen B, Ramos-Esteban J, Podos SM, Mittag T. Cytoarchitecture of the retinal ganglion cells in the rat. Invest Ophthalmol Vis Sci. 2002; 43(3):587–594. [PubMed: 11867571]

De Valois RL, Thorell LG, Albrecht DG. Periodicity of striate-cortex-cell receptive fields. J Opt Soc Am A. 1985; 2(7):1115–1123. [PubMed: 4020508]

DeAngelis GC, Ohzawa I, Freeman RD. Spatiotemporal organization of simple-cell receptive fields in the cat's striate cortex. II. Linearity of temporal and spatial summation. J Neurophysiol. 1993; 69(4):1118–1135. [PubMed: 8492152]

Dong H, Shao Z, Nerbonne JM, Burkhalter A. Differential depression of inhibitory synaptic responses in feedforward and feedback circuits between different areas of mouse visual cortex. J Comp Neurol. 2004; 475(3):361–373. [PubMed: 15221951]

Drager UC. Receptive fields of single cells and topography in mouse visual cortex. J Comp Neurol. 1975; 160(3):269–290. [PubMed: 1112925]

Gilbert CD, Wiesel TN. Columnar specificity of intrinsic horizontal and corticocortical connections in cat visual cortex. J Neurosci. 1989; 9(7):2432–2442. [PubMed: 2746337]

Girman SV, Sauve Y, Lund RD. Receptive field properties of single neurons in rat primary visual cortex. J Neurophysiol. 1999; 82(1):301–311. [PubMed: 10400959]

Grubb MS, Thompson ID. Quantitative characterization of visual response properties in the mouse dorsal lateral geniculate nucleus. J Neurophysiol. 2003; 90(6):3594–3607. [PubMed: 12944530]

Heimel JA, Van Hooser SD, Nelson SB. Laminar organization of response properties in primary visual cortex of the gray squirrel (Sciurus carolinensis). J Neurophysiol. 2005; 94(5):3538–3554. [PubMed: 16000528]

Hensch TK. Critical period plasticity in local cortical circuits. Nat Rev Neurosci. 2005; 6(11):877–888. [PubMed: 16261181]

Hensch TK, Fagiolini M, Mataga N, Stryker MP, Baekkeskov S, Kash SF. Local GABA circuit control of experience-dependent plasticity in developing visual cortex. Science. 1998; 282(5393):1504–1508. [PubMed: 9822384]

Hubel DH, Livingstone MS. Segregation of form, color, and stereopsis in primate area 18. J Neurosci. 1987; 7(11):3378–3415. [PubMed: 2824714]

Hubener M. Mouse visual cortex. Curr Opin Neurobiol. 2003; 13(4):413–420. [PubMed: 12965287]

Johnson RR, Burkhalter A. A polysynaptic feedback circuit in rat visual cortex. J Neurosci. 1997; 17(18):7129–7140. [PubMed: 9278547]

Kalatsky VA, Stryker MP. New paradigm for optical imaging: temporally encoded maps of intrinsic signal. Neuron. 2003; 38(4):529–545. [PubMed: 12765606]

Mangini NJ, Pearlman AL. Laminar distribution of receptive field properties in the primary visual cortex of the mouse. J Comp Neurol. 1980; 193(1):203–222. [PubMed: 6776165]

Maruko I, Zhang B, Tao X, Tong J, Smith EL 3, Chino YM. Postnatal development of disparity sensitivity in visual area 2 (v2) of macaque monkeys. J Neurophysiol. 2008; 100(5):2486–2495. [PubMed: 18753321]

Metin C, Godement P, Imbert M. The primary visual cortex in the mouse: receptive field properties and functional organization. Exp Brain Res. 1988; 69(3):594–612. [PubMed: 3371440]

Morishita H, Hensch TK. Critical period revisited: impact on vision. Curr Opin Neurobiol. 2008; 18(1):101–107. [PubMed: 18534841]

Naka KI, Rushton WA. S-potentials from colour units in the retina of fish (Cyprinidae). J Physiol. 1966; 185(3):536–555. [PubMed: 5918058]

Niell CM, Stryker MP. Highly selective receptive fields in mouse visual cortex. J Neurosci. 2008; 28(30):7520–7536. [PubMed: 18650330]

Ohzawa I, Sclar G, Freeman RD. Contrast gain control in the cat's visual system. J Neurophysiol. 1985; 54(3):651–667. [PubMed: 4045542]

Pelli DG. The VideoToolbox software for visual psychophysics: transforming numbers into movies. Spat Vis. 1997; 10(4):437–442. [PubMed: 9176953]

Prusky GT, West PW, Douglas RM. Behavioral assessment of visual acuity in mice and rats. Vision Res. 2000; 40(16):2201–2209. [PubMed: 10878281]

Rosa MG, Krubitzer LA. The evolution of visual cortex: where is V2? Trends Neurosci. 1999; 22(6): 242–248. [PubMed: 10354599]

Sakai E, Bi H, Maruko I, Zhang B, Zheng J, Wensveen J, Harwerth RS, Smith EL 3, Chino YM. Cortical effects of brief daily periods of unrestricted vision during early monocular form deprivation. J Neurophysiol. 2006; 95(5):2856–2865. [PubMed: 16452254]

Salinas-Navarro M, Mayor-Torroglosa S, Jimenez-Lopez M, Aviles-Trigueros M, Holmes TM, Lund RD, Villegas-Perez MP, Vidal-Sanz M. A computerized analysis of the entire retinal ganglion cell population and its spatial distribution in adult rats. Vision Res. 2009; 49(1):115–126. [PubMed: 18952118]

Schwabe L, Obermayer K, Angelucci A, Bressloff PC. The role of feedback in shaping the extra-classical receptive field of cortical neurons: a recurrent network model. J Neurosci. 2006; 26(36): 9117–9129. [PubMed: 16957068]

Sclar G, Maunsell JH, Lennie P. Coding of image contrast in central visual pathways of the macaque monkey. Vision Res. 1990; 30(1):1–10. [PubMed: 2321355]

Simmons PA, Pearlman AL. Receptive-field properties of transcallosal visual cortical neurons in the normal and reeler mouse. J Neurophysiol. 1983; 50(4):838–848. [PubMed: 6313871]

Skottun BC, De Valois RL, Grosof DH, Movshon JA, Albrecht DG, Bonds AB. Classifying simple and complex cells on the basis of response modulation. Vision Res. 1991; 31(7-8):1079–1086. [PubMed: 1909826]

Sohya K, Kameyama K, Yanagawa Y, Obata K, Tsumoto T. GABAergic neurons are less selective to stimulus orientation than excitatory neurons in layer II/III of visual cortex, as revealed by in vivo functional Ca2+ imaging in transgenic mice. J Neurosci. 2007; 27(8):2145–2149. [PubMed: 17314309]

Solomon SG, Peirce JW, Lennie P. The impact of suppressive surrounds on chromatic properties of cortical neurons. J Neurosci. 2004; 24(1):148–160. [PubMed: 14715948]

Swindale NV. Orientation tuning curves: empirical description and estimation of parameters. Biol Cybern. 1998; 78(1):45–56. [PubMed: 9518026]

Trachtenberg JT, Trepel C, Stryker MP. Rapid extragranular plasticity in the absence of thalamocortical plasticity in the developing primary visual cortex. Science. 2000; 287(5460): 2029–2032. [PubMed: 10720332]

Tropea D, Van Wart A, Sur M. Molecular mechanisms of experience-dependent plasticity in visual cortex. Philos Trans R Soc Lond B Biol Sci. 2009; 364(1515):341–355. [PubMed: 18977729]

van Brussel L, Gerits A, Arckens L. Identification and localization of functional subdivisions in the visual cortex of the adult mouse. J Comp Neurol. 2009; 514(1):107–116. [PubMed: 19260069]

Van der Gucht E, Hof PR, Van Brussel L, Burnat K, Arckens L. Neurofilament protein and neuronal activity markers define regional architectonic parcellation in the mouse visual cortex. Cereb Cortex. 2007; 17(12):2805–2819. [PubMed: 17337746]

Van Hooser SD. Similarity and diversity in visual cortex: is there a unifying theory of cortical computation? Neuroscientist. 2007; 13(6):639–656. [PubMed: 17911223]

Van Hooser SD, Heimel JA, Chung S, Nelson SB. Lack of patchy horizontal connectivity in primary visual cortex of a mammal without orientation maps. J Neurosci. 2006; 26(29):7680–7692. [PubMed: 16855096]

Van Hooser SD, Heimel JA, Chung S, Nelson SB, Toth LJ. Orientation selectivity without orientation maps in visual cortex of a highly visual mammal. J Neurosci. 2005; 25(1):19–28. [PubMed: 15634763]

Van Hooser SD, Nelson SB. The squirrel as a rodent model of the human visual system. Vis Neurosci. 2006; 23(5):765–778. [PubMed: 17020632]

Wagor E, Mangini NJ, Pearlman AL. Retinotopic organization of striate and extrastriate visual cortex in the mouse. J Comp Neurol. 1980; 193(1):187–202. [PubMed: 6776164]

Walker GA, Ohzawa I, Freeman RD. Suppression outside the classical cortical receptive field. Vis Neurosci. 2000; 17(3):369–379. [PubMed: 10910105]

Wang Q, Burkhalter A. Area map of mouse visual cortex. J Comp Neurol. 2007; 502(3):339–357. [PubMed: 17366604]

Xing D, Ringach DL, Shapley R, Hawken MJ. Correlation of local and global orientation and spatial frequency tuning in macaque V1. J Physiol. 2004; 557(Pt 3):923–933. [PubMed: 15090603]

Zhang B, Zheng J, Watanabe I, Maruko I, Bi H, Smith EL 3, Chino Y. Delayed maturation of receptive field center/surround mechanisms in V2. Proc Natl Acad Sci U S A. 2005; 102(16): 5862–5867. [PubMed: 15824308]

Zheng J, Zhang B, Bi H, Maruko I, Watanabe I, Nakatsuka C, Smith EL 3, Chino YM. Development of temporal response properties and contrast sensitivity of V1 and V2 neurons in macaque monkeys. J Neurophysiol. 2007; 97(6):3905–3916. [PubMed: 17428899]

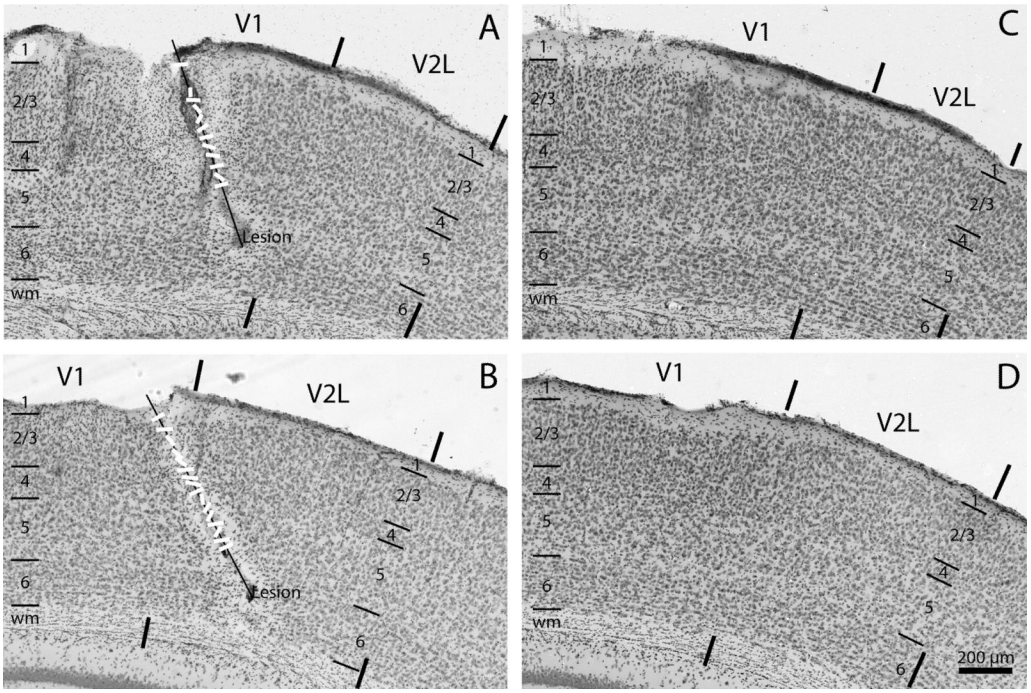

Figure 1.

Reconstruction of electrode tracks and recording sites in V1 (A) and V2L (B) in mouse visual cortex. Adjacent sections where the electrode track and lesions were not visible are shown in C and D. Layers are easily identifiable and indicated on the left and right. Electrolytic lesions at the end of penetrations are labeled. Preferred orientation of each unit is also indicated by a short bar. Note that in V1 (A), there were two penetrations and the second penetration that was made perpendicular to the surface ended in layer 4. The penetration in panel B shows that the majority of units were from V2L except the first 3 units that were in V1. WM signifies the white matter. The markers indicate the location of the borders between V1 and V2L and V2L and auditory cortex. V1 could be distinguished from V2L by its thicker layer 4 and a less densely packed layer 5, in particular immediately above layer 6 where a sublayer with fewer cells is visible in V1 but not V2L.

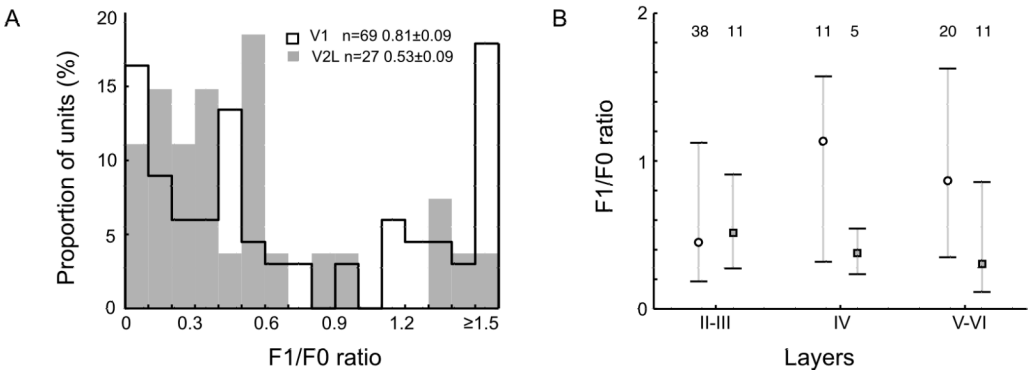

Figure 2.

(A) Frequency distributions of F_1/F_0 ratios for mouse cell population (n=96). Cells with the ratio ≥ 1.0 were classified as simple cells and those having the ratio < 1.0 were classified as complex cells (Skottun et al., 1991). The frequency distribution for V1 cells is indicated by open bars (n=69), for V2L cells by filled bars (n=27). (B) Layer differences in F_1/F_0 ratio in mouse V1 (open circles) and V2L (closed squares). Circles or squares indicate the median values while short bars indicate quartile values. The number at the top indicates the number of units for each group.

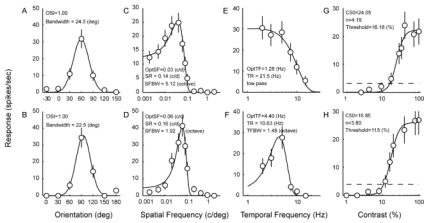

Figure 3.

Representative tuning curves for stimulus orientation (A-B), spatial frequency (C-D), temporal frequency (E-F), and contrast (G-H) in mice.

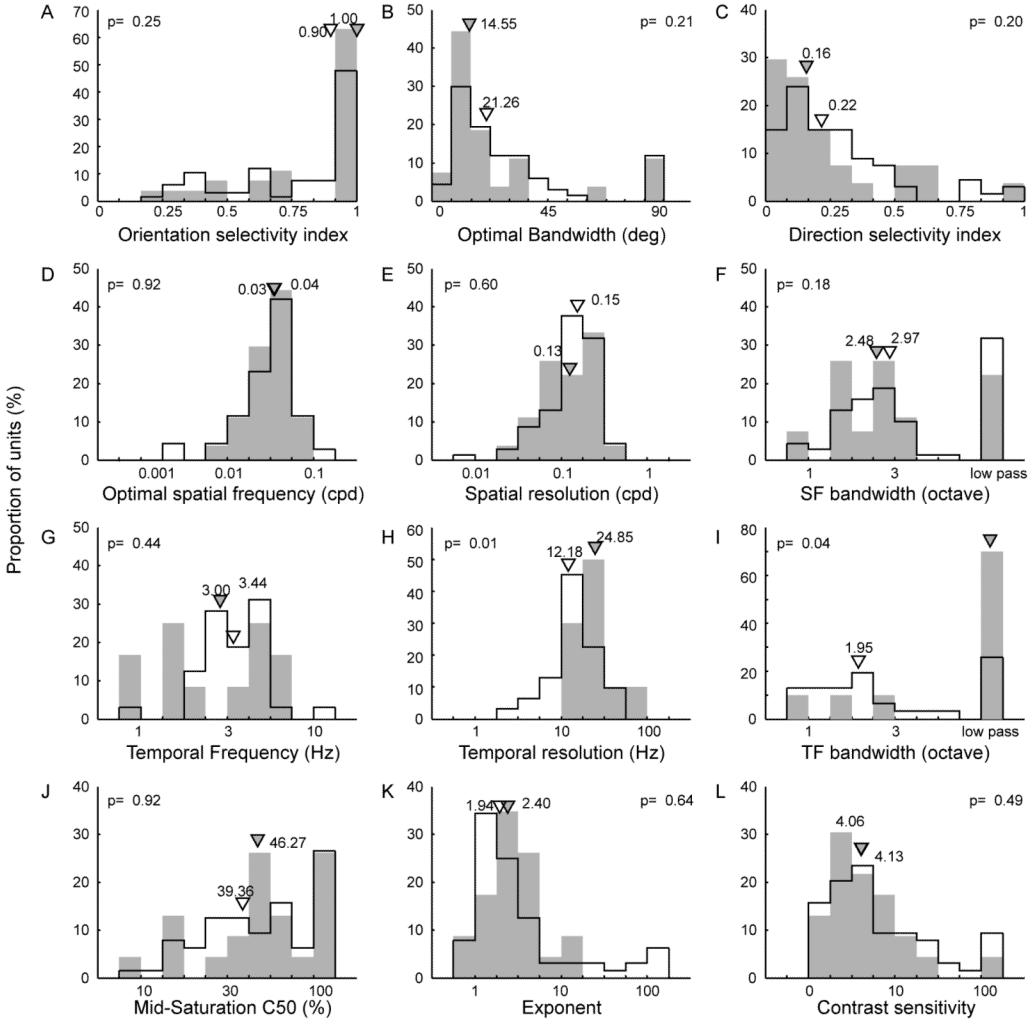

Figure 4.

Frequency distributions of spatial and temporal response properties and contrast sensitivity of V1 and V2L neurons in mice. Histograms of orientation/direction selectivity (A-C), spatial frequency selectivity (D-F), temporal frequency selectivity (G-I), and contrast sensitivity (J-L). In each panel, open bars indicate V1 neurons and filled bars represent V2L neurons with corresponding triangles indicating median values.

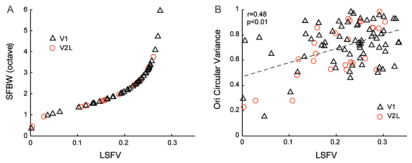

Figure 5.

Relationships between response attenuation at low spatial frequency (LSFV) and spatial frequency bandwidth (A) and circular variance (CV) (B) in mice. V1 neurons are shown in black triangles, V2L units by red circles.

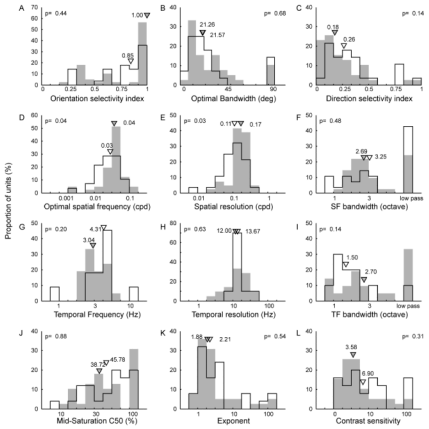

Figure 6.

Frequency distributions of spatial and temporal response properties and contrast sensitivity of simple and complex cells of V1 and V2L neurons in mice. Histograms of orientation/direction selectivity (A-C), spatial frequency selectivity (D-F), temporal frequency selectivity (G-I), and contrast sensitivity (J-L). In each panel, open bars indicate simple cells and filled bars represent complex cells with corresponding triangles indicating median values.

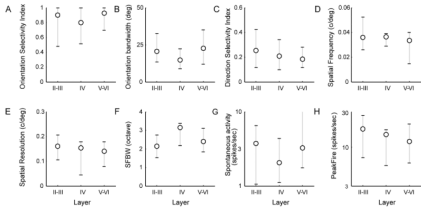

Figure 7.

Layer differences in orientation (A-C) and spatial frequency tuning (D-F) and spontaneous (G) and peak (H) firing rates in mice. Circles indicate the median values and short bars indicate quartile values. The sample size for each layer group is the same as that in Fig 2B.

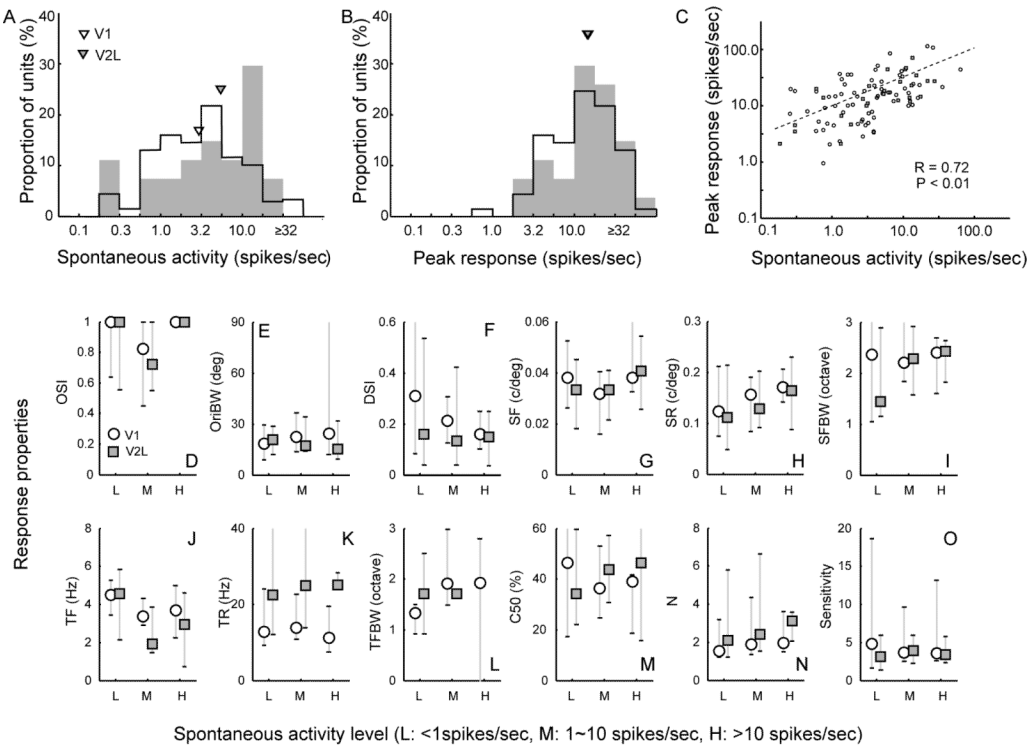

Figure 8.

Relationships between the spontaneous activity and the peak firing rate, spatial and temporal tuning properties and contrast sensitivity of mouse V1 and V2L neurons. Frequency distribution of spontaneous activity of V1 (open bars) and V2L (Filled bars) neurons (A), and peak firing rate (B). Peak firing rate as a function of spontaneous activity in V1 (open circle) and V2L (open square) (C). Spatial and temporal tuning properties and contrast sensitivity (D-O) as a function of spontaneous firing rates. Cells were arbitrarily divided into low (sp < 1.0 spikes/sec), middle (1.0 < sp < 10.0 spikes/sec, and high (sp > 10/spikes/sec) spontaneous groups.

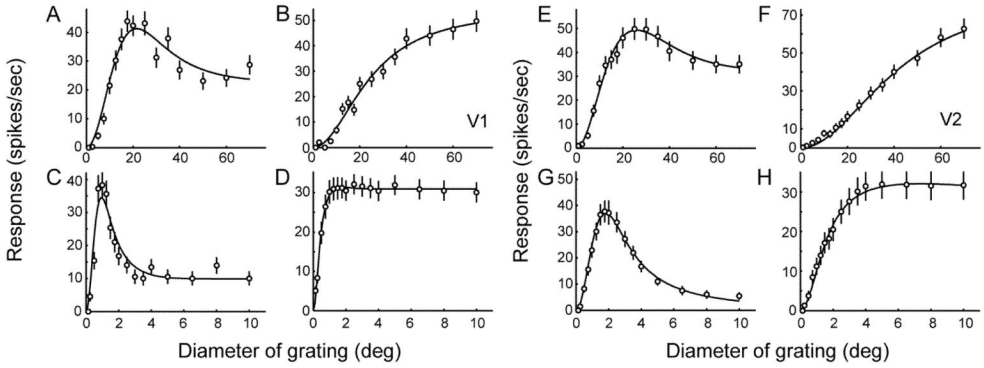

Figure 9.

Representative size tuning functions of V1 (A-D) and V2 neurons (E-H) in mice (top: A,B,E,F) and macaque monkeys (bottom: C,D,G,H). Data points were fitted with the ratios of Gaussians (Cavanaugh et al., 2002). For each species, units with and without surround suppression are illustrated.

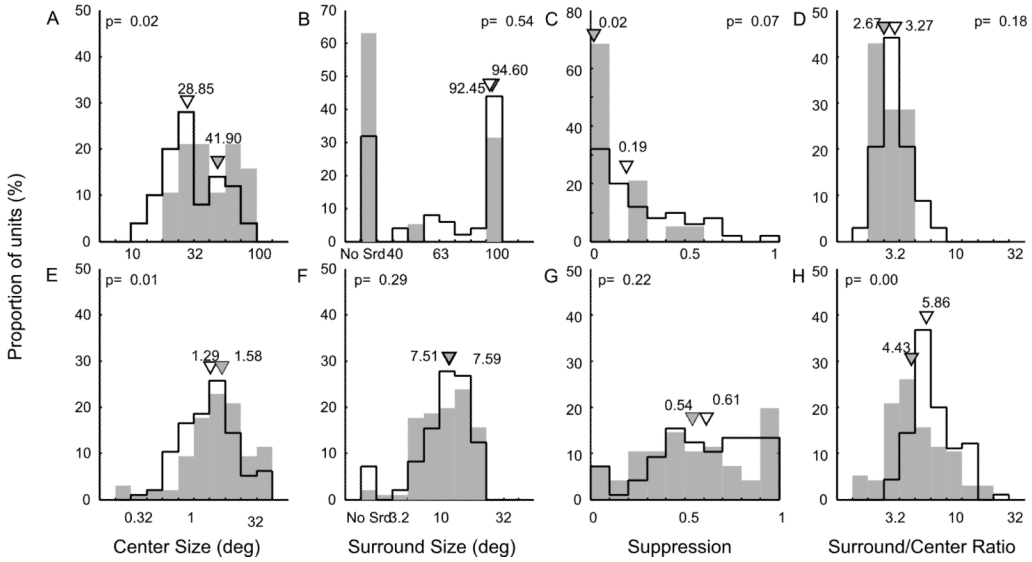

Figure 10.

Receptive field center and surround properties of V1 and V2 neurons in mice and monkeys. Frequency distribution of V1 (open bars) and V2 (filled bars) neurons of RF center size (A), surround size (B), suppression index (C) and surround/center size ratio (D) in mouse visual cortex. Triangles indicate median values. Frequency distributions of center size (E), surround size (F), suppression index (G) and surround/center size ratio (H) in monkeys. *No Srd* signifies those neurons without measurable RF surrounds.

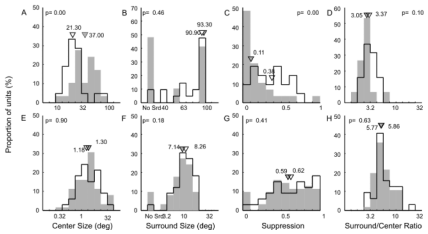

Figure 11.

Receptive field center and surround properties of V1 and V2 neurons in mice and monkeys. Frequency distribution of simple cells (open bars) and complex cells (filled bars) of RF center size (A), surround size (B), suppression index (C) and surround/center size ratio (D) in mouse visual cortex. Triangles indicate median values. Frequency distributions of center size (E), surround size (F), suppression index (G) and surround/center size ratio (H) in monkeys. *No Srd* signifies those neurons without measurable RF surrounds.

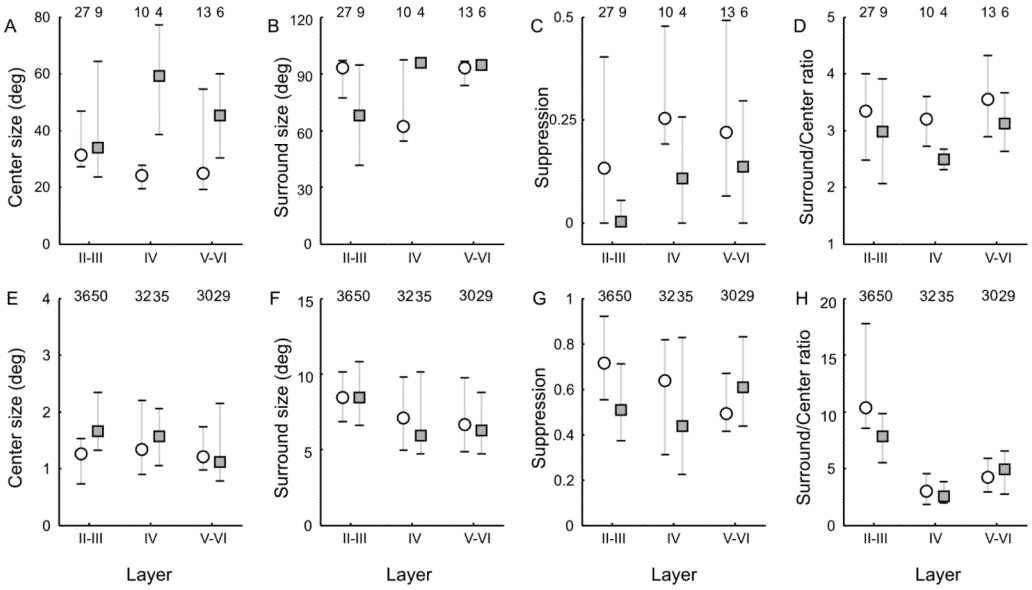

Figure 12.

Correlation between the strength of RF surround suppression (SI) and RF center size (A), surround size (B), and surround/center size ratio (C) of individual neurons in mice (red) and monkeys (black). Triangles signify V1 neurons and circles indicate V2 neurons. Dotted lines with r-values indicate fit for mice and continuous lines with r-values indicate fit for monkeys.

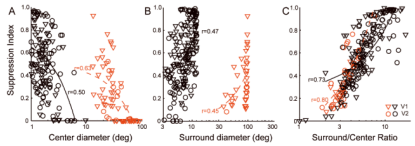

Figure 13.

Layer differences in center size (A, E), surround size (B, F), suppression index (C, G) and surround/center size ratio (D, H) in mice (A-D) and monkey (E-H). Circles and squares indicate the median values of V1 and V2L units respectively and short bars indicate quartile values. Numbers of units per layer and brain region are indicated on top.

Table 1

Summary of the mean (± se) values for selectivity for stimulus orientation, spatial frequency, temporal frequency, size and contrast of V1 and V2 neurons in mice and macaque monkeys

	V1		V2	
	Mouse	**Monkey**	**Mouse**	**Monkey**
Orientation tuning				
Orientation bandwidth (deg)	22.15±1.63	20.28±2.35	18.43±2.54	22.84±2.54
Direction selectivity	0.27±0.03	0.45±0.06	0.23±0.05	0.53±0.08
Spatial frequency tuning				
Optimal SF (c/deg)	0.04±0.002	2.43±0.22	0.04±0.0015	2.69±0.65
Spatial resolution (c/deg)	0.15±0.01	9.83±0.78	0.15±0.02	9.68±0.42
SF bandwidth (octave)	2.38±0.15	2.54±0.24	2.11±0.17	2.67±0.32
Temporal frequency tuning				
Optimal TF (Hz)	3.79±0.34	5.09±0.33	3.06±0.63	5.23±0.31
Temporal resolution (Hz)	15.39±1.57	19.85±1.17	26.22±4.43	18.76±1.04
TF bandwidth (octave)	1.97±0.27	3.08±0.12	1.71±0.46	2.92±0.12
Contrast tuning				
C50 (%)	42.47±3.29	24.59±1.56	43.41±5.09	19.51±1.52
N	6.86±2.19	3.05±0.19	3.72±0.78	3.61±0.36
Threshold (%)	11.13±3.82	8.63±0.60	18.30±3.94	10.70±1.12
Size tuning				
Center size (deg)	34.93±2.63	1.28±0.11	47.13±4.75	1.77±0.11
Surround size (deg)	81.66±3.44	7.96±0.26	87.40±7.64	7.52±0.29
Suppression	0.24±0.035	0.59±0.03	0.11±0.04	0.55±0.04
Surround/Center Ratio	3.46±0.18	7.01±0.33	2.91±0.26	5.46±0.34